agronomy

MDPI

Article

Foliar Application of Humic-Stabilized Nanoferrihydrite Resulted in an Increase in the Content of Iron in Wheat Leaves

Mariya M. Zimbovskaya [1], Alexander Yu. Polyakov [2,3], Dmitry S. Volkov [1,4], Natalia A. Kulikova [1,5,6], Vasily A. Lebedev [1], Denis A. Pankratov [1], Andrey I. Konstantinov [1], Aksana M. Parfenova [1], Oral Zhilkibaev [7,8] and Irina V. Perminova [1,*]

1 Department of Chemistry, Lomonosov Moscow State University, Leninskiye Gory 1-3, 119991 Moscow, Russia; anuchina_mariya@mail.ru (M.M.Z.); dmsvolkov@gmail.com (D.S.V.); knat@darvodgeo.ru (N.A.K.); vasya_lebedev@mail.ru (V.A.L.); pankratov@radio.chem.msu.ru (D.A.P.); konstant@med.chem.msu.ru (A.I.K.); parf@colloid.chem.msu.ru (A.M.P.)

2 Department of Materials Science, Lomonosov Moscow State University, Leninskiye Gory 1-73, 119991 Moscow, Russia; a.yu.polyakov@gmail.com

3 Industrial Focus Group XUV Optics, MESA+ Institute of Nanotechnology, University of Twente, Drienerlolaan 5, 7522 NB Enschede, The Netherlands

4 Department of Chemistry and Physical Chemistry of Soils, V.V. Dokuchaev Soil Science Institute, Pyzhyovskiy Lane 7 Build. 2, 119017 Moscow, Russia

5 Department of Soil Science, Lomonosov Moscow State University, Leninskiye Gory 1-12, 119991 Moscow, Russia

6 Bach Institute of Biochemistry, Fundamentals of Biotechnology Federal Research Center, Russian Academy of Sciences, pr. Leninskiy 33, 119071 Moscow, Russia

7 Department of Chemistry, Al Farabi Kazakh National University, 71 Al-Farabi Ave., Almaty 050040, Kazakhstan; zhilkibaevoral@mail.ru

8 InterAgroTech LLC, Almaty 0500040, Kazakhstan

* Correspondence:iperm@med.chem.msu.ru; Tel.: +7-495-939-55-46

Received: 1 November 2020; Accepted: 27 November 2020; Published: 29 November 2020

Abstract: The objective of this study was to synthesize iron (hydr)oxide nanoparticles (IONPs) stabilized by humic substances, and to estimate the feasibility of their use for foliar application on iron deficient plants. The IONPs were synthesized by rapid hydrolysis of iron(III) nitrate in a solution of potassium humate. The iron speciation and nanoparticle morphologies were characterized using X-ray diffraction, transmission electron microscopy, and Mössbauer spectroscopy. The obtained sample of IONPs was applied at concentrations of 1- and 10-mM Fe, and 0.2% urea was used as an adjuvant. Wheat plants (*Triticum aestivum* L. cv. L15) were used for the iron uptake test. For both of the concentrations tested, spraying the nanoparticles resulted in a 70–75% higher iron content in wheat leaves compared to ferric ammonium salt of ethylenediaminetetraacetic acid (Fe-EDTA). The synergistic effect of humic substances acting as a surfactant seemed to promote an increase in the iron uptake of the ferrihydrite nanoparticles compared to the aqueous Fe-EDTA solution used in this study. We concluded that humic-stabilized IONPs are much better suited to foliar application as compared to soil amendment when applied as a source of iron for plants. This is because humic substances act as a capping agent for nanoparticles and the surfactants enhance iron penetration into the leaf.

Keywords: humic substances; capping agents; ferrihydrite; nanoparticles; iron deficiency; nutrition; biofortification; foliar application; wheat

1. Introduction

Fe deficiency is a frequent issue in numerous crops, particularly in calcareous soils [1,2]. This is because of the poor bioavailability of Fe, which produces insoluble Fe(III) oxides and oxohydroxides in soil [3,4]. At the same time, iron (hydr)oxide nanoparticles (IONPs) measuring < 5–20 nm are the most frequently used as iron-containing nanofertilizers [5–8]. Bare IONPs are prone to aggregation due to their high surface energy; this tendency is more pronounced near the point of zero charge (PZC), which usually ranges between pH 7 and 9 for synthetic iron oxides [9], and at elevated salt concentrations [10]. Among the different ligands used for nanoparticle stabilization, humic substances (HS) deserve particular attention as they are eco-friendly natural polyelectrolytes. HS stabilize iron (hydr)oxides in soils [11–13], and they are widely used for stabilization of synthetic IONPs [10,14–16]. Substantial efforts have been undertaken in the last decade to combine the benefits of HS and IONPs in designing eco-friendly nanofertilizers [6,8,17–20] that meet the demands of sustainable chemistry [21]. Despite the progress made in this area, and well documented increases in iron uptake by plants, the efficacy of HS-based iron nanofertilizers remains much lower compared to that of iron chelates. The main reason is aggregation of HS-stabilized IONPs on the root surface upon soil application as well as interaction with soil particles [22,23].

Foliar application of micronutrients, including their nano-forms is an advanced fertilization technology that has great potential for the production of nutritious and safe foods [24–31]. It also provides a more efficient route for the application of nanoparticles, whose bioavailability is much higher when applied via leaf sprays as compared to soil amendments, as has been shown in two recent reviews [22,23]. Comparative investigations of nanoparticle delivery to plants by foliar versus soil applications have indicated that leaf spraying has significant advantages for nanoscale nutrient uptake [32,33]. This effect was consistent for different crops including brown rice [34], wheat grain [35], soybean (*Glycine max* (L.) Merr.) [32], and black-eyed peas [36].

Numerous reports have shown the benefits of foliar application for both soluble forms of micronutrients and for nanoparticles [37–41]. HS were used for improving iron uptake upon foliar application of Fe-chelates [42,43]. Moreover, complexes of Fe-HS [44] and Fe-lignosulfonate [45] were successfully tested as foliar iron fertilizers. However, so far, we have not found reports on the foliar application of HS-stabilized IONPs. The combination of surface-active HS and IONPs is expected to be particularly beneficial for the foliar spray, which requires improved wettability of a moderately hydrophobic leaf surface and strong adhesion of the fertilizing component. According to a recent study [46], the combined particle-and-surfactant systems exhibited (i) a decreasing contact angle along with increasing nanoparticle concentration, and (ii) a much lower wetting angle than that of the only-surfactant system at the same surfactant concentration (in the whole range of nanoparticle concentrations studied). Mixtures of surface-active nanoparticles and surfactants also stabilize the liquid–liquid interface in emulsions [47] applied in the oil industry [48] and commercial formulations including agrochemical suspoemulsions [49]. Therefore, humic-stabilized IONPs might be suited for the droplet design of foliar spraying.

The objective of this study was to synthesize humic-stabilized IONPs and to estimate iron uptake as compared to ferric ammonium salt of ethylenediaminetetraacetic acid (Fe-EDTA) upon foliar application on wheat plants (*Triticum aestivum* L. cv. L15).

2. Materials and Methods

2.1. Humic Material Characterization

Potassium humate ("Sakhalin Humate", Moscow, Russia) was used as the humic source material and designated as CHS-K. The elemental composition of CHS-K was determined using a Vario MicroCube elemental analyzer (Elementar, Langenselbold, Germany). The contents of the elements were (%, mass): C—32, H—2.8, N—1.3. The ash content was 22.9%. The contents of the elements on an ash-free basis were (% wt): C—47.1, H—3.63, N—1.69, O—47.58. The corresponding atomic ratios were: H/C—1.05, O/C—0.76, C/N—28.8. The values of H/C and O/C ratios obtained for CHS-K are indicative of a low degree of condensation and high oxidation of this humic material, which is typical

for the low-ranked oxidized coal used for its extraction. The structural-group composition of CHS-K was determined using a ^{13}C NMR spectrometer Avance 400 (Bruker, Ettlingen, Germany) operating at ^{13}C nuclei frequency of 100 MHz. A weight of 40 mg of CHS-K was dissolved in 0.6 mL of 0.3 M NaOD/D_2O. The conditions for quantitative measurement of the C distribution as well as the spectral assignments were made as described elsewhere [50,51]. The content of C in different chemical environments was as follows (% of total C): aliphatic non-substituted C (C_{alk})–11.9; aliphatic (O,N)-substituted C ($C_{Alk\text{-}O,N}$)–6.9; aromatic non-substituted C (C_{Ar})–43.6; aromatic O,N -substituted C ($C_{Ar\text{-}O,N}$)–9.7; carboxyl and ester groups ($C_{COO\text{-}H,R}$)–19.5; C of quinone and ketone groups ($C_{C=O}$)–6.8. The measured values agreed well with the literature data for coal HS, which are enriched with aromatic carbon and carboxyl groups [52]. The molecular weight distribution of CHS-K was determined using size exclusion chromatography (SEC) as described by Perminova et al. (1998) [53]. The chromatography system Abimed (Gilson, Paris, France) included an HPLC pump, an autosampler, a glass column (diameter of 15 mm, length of 25 cm), a UV spectrophotometric detector, and a recording computer. The column was filled with a Toyopearl TSK HW-55S gel (Toso-Haas, Tokyo, Japan) with a fractionation range of 1–200 kDa (as for polydextrans). A phosphate buffer (0.03 M, pH 6.8) was used as a mobile phase. The determined number-averaged (M_n) and weight-averaged (M_w) molecular weights and M_w/M_n ratio (polydispersity) were 3.2 kDa, 12.0 kDa, and 3.7, respectively. They are in good agreement with the MW data obtained with the use of SEC for the other coal HS [54].

2.2. The Iron Sources

Ethylenediaminetetraacetic acid iron chelate (Fe-EDTA) (BASF AG, Germany) was used as a reference iron chelate. Ferrihydrite NPs (FH) were prepared as follows. A weight of 3.5 g of CHS-K was dissolved in 400 mL of deionized water in a round-bottom flask and 1-2 mL of 3 M KOH was added to improve humate dissolution; the final pH was 11.2. A weight of 2.53 g of $Fe(NO_3)_3{\cdot}9H_2O$ was dissolved in 25 mL of deionized water. The obtained 0.25 M $Fe(NO_3)_3$ solution was added as droplets to the humate solution under continuous stirring until a pH of 10 was attained. Then, 3 M KOH was added simultaneously with $Fe(NO_3)_3$ to maintain pH 10. The pH fluctuations during the synthesis were in the range of 9.7 to 10.3. After the addition of the full volume of $Fe(NO_3)_3$ solution, the reaction mixture was diluted up to 500 mL by deionized water and the pH set to 10. The final solution contained 7 g/L of humate and 25 mM of Fe in the form of ferrihydrite (FH) (~10% Fe (wt) on the dry weight of FH). For the bioassay, the obtained FH solution was diluted to achieve 1 mM and 10 mM Fe concentrations. As described below, urea (0.2% wt.) was added to the FH solution before its application to the plants.

2.3. Characterization of the Iron Source (FH) Used in this Study

Mössbauer spectroscopy was used to study speciation of Fe in the obtained sample of FH (10 mM Fe). Two FH aliquots (25–30 mL, with or without urea) were dried at 45 °C until a constant weight. The obtained dry product was ground and placed in an evacuated cryostat using a plastic cuvette. Mössbauer spectra were obtained using a MS1104EM Express Mössbauer spectrometer (Cordon GmbH, Rostov-on-Don, Russia). The radiation source was ^{57}Co in a metal rhodium matrix with an activity of 2 mCi (RITVERC GmbH, St. Petersburg, Russia). The spectra were obtained both at room temperature (298 ± 3 K), and at a liquid N_2 temperature (77.5 ± 0.5 K). The spectra were collected until the noise/signal ratio decreased down to ≤ 1%. The high-resolution (1024 points) experimental Mössbauer spectra were processed using SpectrRelax 2.4 software (Lomonosov MSU, Moscow, Russia). The isomer shifts were determined relative to α-Fe.

Transmission electron microscopy (TEM) was performed using a Zeiss Libra 200 MC microscope (Zeiss, Oberkochen, Switzerland), equipped with a monochromator and an Omega-filter. The suspension of FH sample was prepared in distilled water by sonication for 3 min and dripped onto the lacey-carbon-coated TEM grid. After 1 min, the excess solution was removed to reduce the amount of soluble mineral salts. The electron diffraction (ED) patterns of raw potassium humate and

the synthesized IONPs were subjected to radial integration using Gwyddion software v. 2.52 [55] followed by polynomial background removal using in-house Python scripts.

To measure the contact angles, the wheat leaves fragments (ca. 2 × 2 cm) were horizontally fixed on the microscope slide glass, a droplet of 20 μl of either distilled water, or Fe-EDTA, or CHS-K, or FH solutions, were placed onto the leaf surface (the FH suspension was rigorously shaken for several minutes before this procedure). All solutions contained urea adjuvant (0.2% wt.). The contact angles were measured by the static sessile drop method. Two μl colloid or distilled water droplets were placed on the horizontally fixed wheat leaf. The images of droplets were captured after 3 s by a horizontal microscope (controlled by iuVCR v. 0.14.0.63 software) and then analyzed using Promer, a custom software designed by the Chair of Colloid Chemistry, Department of Chemistry, Lomonosov MSU. The contact angles were measured at both sides of three droplets and the values were averaged. For each type of solution, measurements were made for five samples.

Surface tension measurements were carried out at room temperature by a maximum bubble pressure method using MP-1 maximum pressure detector. Distilled water was used as a reference fluid. Three measurements were averaged for each sample. For each type of solution, measurements were made for six samples.

2.4. Experiments with Plants

Wheat plants were cultivated from seeds, *Triticum aestivum* L. cv. L15, which originated from the Russian State Agrarian University, Moscow Timiryazev Agricultural Academy. The seeds were surface-sterilized by immersion in 8% hydrogen peroxide for 15 min in the light. After rinsing 5 times with triple-distilled water according to [56], the wheat seeds were left for germination in the dark at 24 °C for 72 h. Then, the germinated seedlings were transferred into 0.5 L polyethylene tanks containing Fe-free Knop nutrient solution (0.14 g·L^{-1} KH_2PO_4, 0.1 g·L^{-1} KCl, 0.14 g·L^{-1} KNO_3, 1.42 g·L^{-1} $MgSO_4 \cdot 7H_2O$, 4.88 g·L^{-1} $Ca(NO_3)_2 \cdot 12H_2O$, pH 5.5) and cultivated in a growth chamber (12 h light/12 h dark photoperiod, illumination 200 μmol m^{-2} s^{-1}; 24 °C) for 21 d.

In this study, Fe-EDTA and FH solutions were used as the iron sources for the foliar treatment at two Fe concentrations: 1 mM Fe and 10 mM Fe. Urea was added to all solutions at a concentration of 0.2% wt. as an adjuvant for increasing the penetration of Fe into the plant based on the literature reports [57,58]. The wheat seedlings (21 d old) were transferred into 0.5 L polyethylene tanks containing Fe-free Knop nutrient solution. Iron was supplied to plants by spraying 5 mL of each iron source solution onto the leaves of 15 wheat plants. Distilled water and the parent potassium humate (with urea) were applied as a control treatment. Clear glass sprayer with aluminum fine mist nozzle pump (Hydior, China) was used for spraying. Seven days after the treatment, the roots and shoots were gently separated; caryopsis and the lower 1.5 cm part were also removed from the shoots. To remove adsorbed iron form the leave surfaces, the shoots were washed for 30 s with the solution of (0.1% HCl/0.01% non-ionic detergent solution, Brij 35) as proposed in [57] and rinsed twice with triple-distilled water. The washed biomass was dried at 24 °C for 14 days (until the weight was constant), weighted, and then subjected to a mineral profile analysis. The washing solutions were analyzed for iron content. All experiments were run in a five-fold biological repetition.

Inductively coupled plasma atomic emission spectroscopy (ICP-AES) was employed to analyze the element content in the iron fertilizers. An axial ICP-AES 5100 spectrometer with an SPS4 autosampler (Agilent Technologies, USA) was used for the liquid sample analysis. For the iron content analysis, the working solution of the FH fertilizer was dried at 45 °C until a constant weight was achieved. Then, 50.00 ± 0.1 mg was placed into a polypropylene flask with a volume of 50.00 ± 0.12 mL, deionized water was added, and mixed. The obtained FH suspensions were treated in a GRAD 28–35 ultrasonic bath (Grad-Technology, Russia) for 0.5 h. These solutions were analyzed directly. For the acid digestion of plants, dried leaf biomass was placed into a digestion tube of a Velp DK 20 digestor (Velp, Spain) with 5 mL of H_2SO_4 (98%, ACS-ISO grade, Panreac) and 4 mL of H_2O_2 (33% USP, pharma grade, AppliChem). The tubes were heated for 30 min at 200 °C, then1 mL of H_2O_2 was added and heated for 30 min at 300 °C. Then, the content of the tubes was transferred into 50 mL polypropylene Sarstedt tubes, diluted with deionized water to a 25 mL mark, and analyzed.

Statistical data treatment included testing the differences between the average values with a one-way analysis of variance (ANOVA). A least significant difference test (LSD) was used for comparisons between means at $p < 0.05$.

3. Results and Discussion

3.1. Characterization of the Synthesized Iron-Containing Nanoparticles

TEM images of the HS-stabilized IONPs synthesized in this study are shown in Figure 1. The numerous ultrafine nanoparticles can be seen within darker regions, which correspond to the amorphous background of HS (Figure 1a). It should be noted that no NPs were detected outside these HS-related areas. This might be indicative of encapsulation of the synthesized ultra-dispersed NPs by the HS matrix. This is feasible, given both the significant excess of potassium humate over the iron precursor (ca. 1:10 Fe/HS mass ratio) used for the reaction and the reported high HS affinity to the surface of iron (hydr)oxides [59]. The size of NPs ranged from 1 to 7 nm with a mean value of (2.5 ± 0.3) nm (Figure 1b), which is typical for HS-stabilized ferrihydrites [19]. For identification of the iron phase in the detected NPs, the normalized plots of integrated ED and background-subtracted ED were calculated as shown in Figure 1c and 1d, respectively. The presence of peaks at 0.15 nm and 0.25 nm in ED of the synthesized FH samples is indicative of nanocrystalline two-line ferrihydrite [60,61]. The two-line ferrihydrite is the least crystalline variety of ferrihydrite family, which falls between the well-defined phases of crystalline iron oxides and short-range ordered ferric polymers [62,63]. Given that a 2-nm ferrihydrite NP is composed of just ~30-unit cells, its lattice is prone to surface relaxation, strain, and disorder [64]. The poor crystallinity of two-line ferrihydrite and high distortion of the lattice make it more amenable to iron release, which is important for the iron source for plant nutrition.

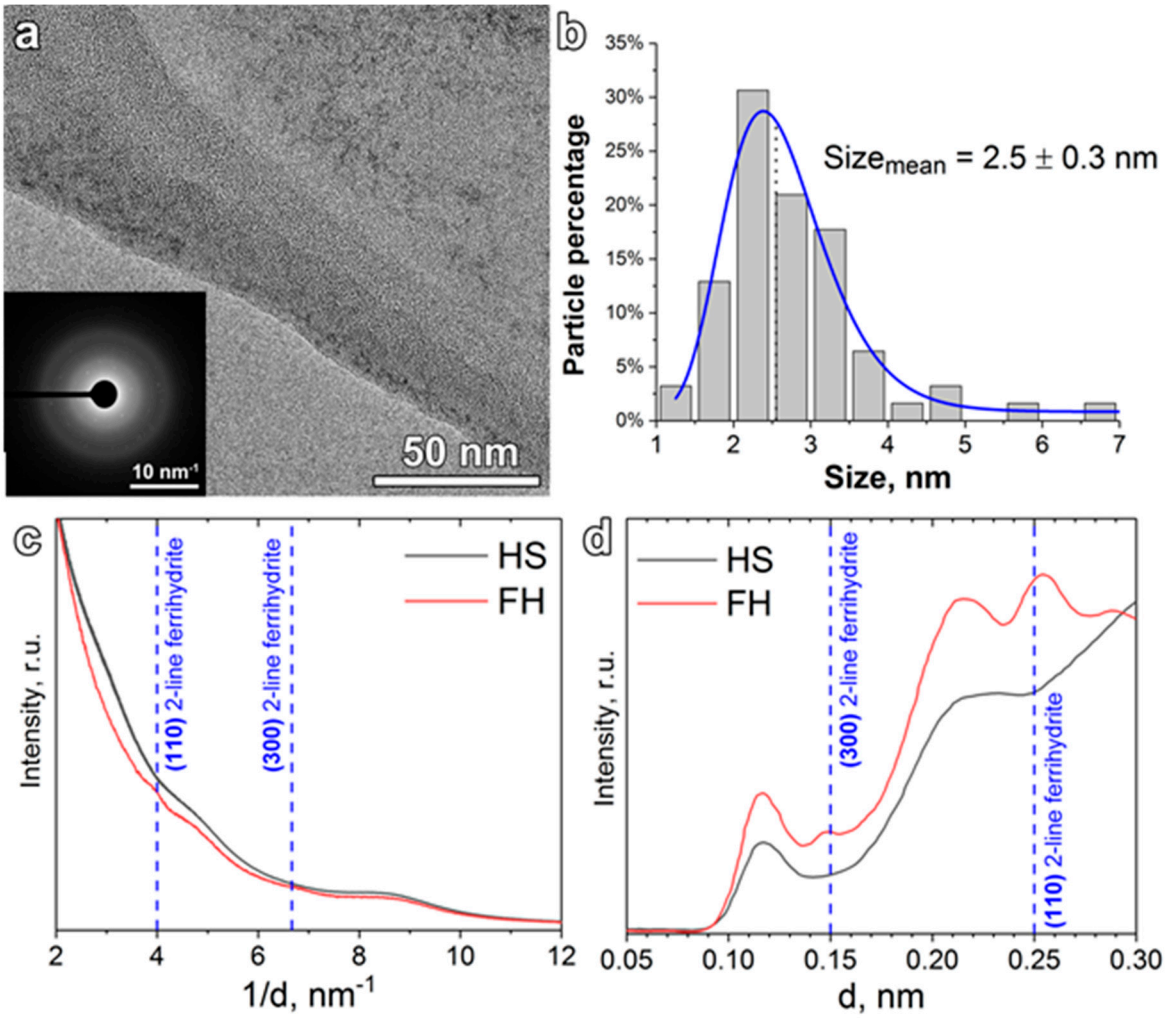

Figure 1. (**a**) TEM image of the synthesized ferrihydrite (FH) nanoparticles and the corresponding electron diffraction image (inset); (**b**) size distribution of nanoparticles in FH nanoparticles as revealed by TEM (log-normal fitting was used); (**c**) normalized electron diffraction integrals for the FH nanofertilizer and raw potassium humate (HS) (d is an interplane lattice spacing); (**d**) normalized background-subtracted electron diffraction of FH nanoparticles and raw potassium humate, replotted in d-space. Positions of the 2-line ferrihydrite reflections and lattice indexes assignments are given according to [60].

The Mössbauer spectra of the dried FH sample were characterized by an asymmetric shape and broadened doublet lines at both room temperature and the boiling point of liquid N_2 (Figure 2a,b). From a non-model description of these spectra, we obtained the probability distribution functions for isomeric shifts and quadrupole splitting (Figure 2c,d). These distributions were characterized by an asymmetric monomodal shape and high dispersion. Both spectra could be satisfactorily fitted with a set of three modes of different width and intensity (Figure 2c,d). This provided the justification for model fitting of the experimental spectra with a set of only three dublet subspectra (Figure 2a,b; Table 1).

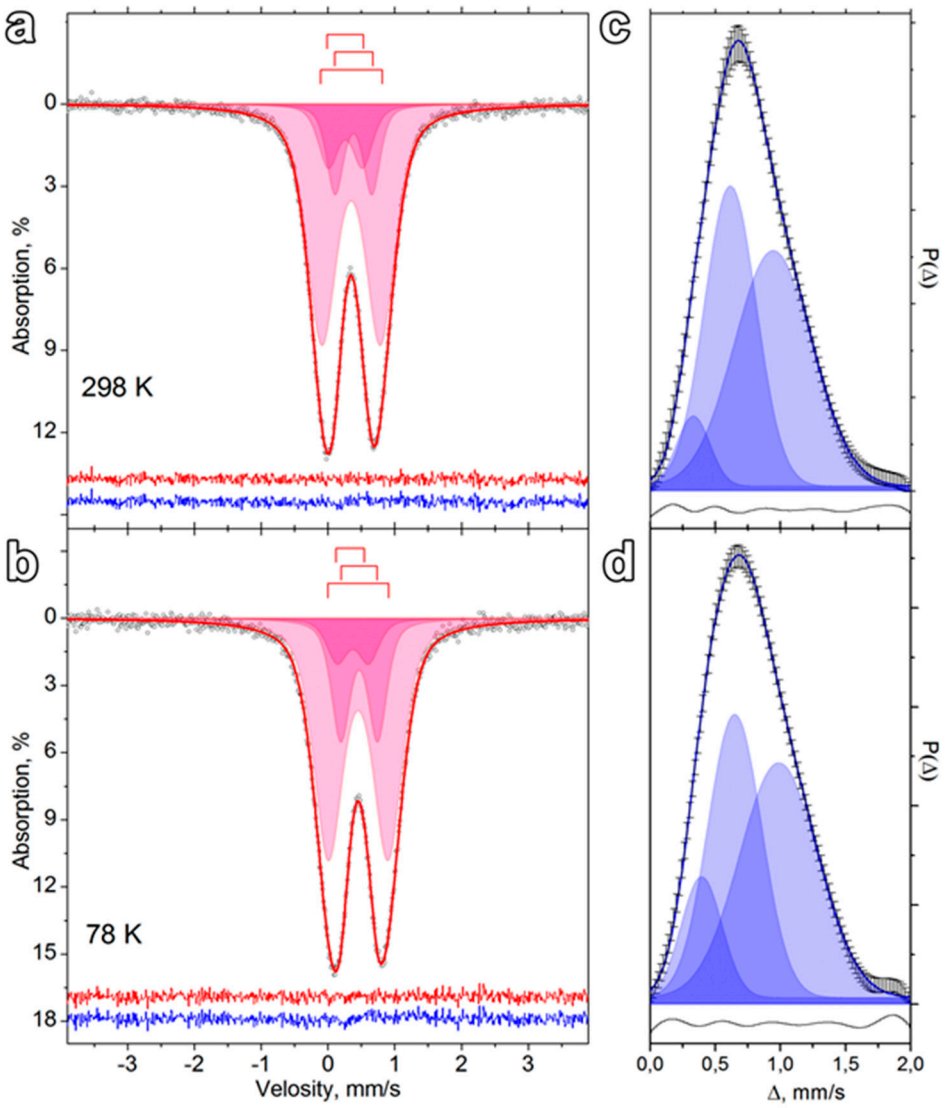

Figure 2. Mössbauer spectra at different temperatures of the ferrihydrite (FH) sample without urea treatment, models for their description (**a**,**b**), and the corresponding quadrupole splitting probability distribution functions (**c**,**d**).

Table 1. The Mössbauer spectroscopy data for the ferrihydrite (FH) nanoparticles in the absence and presence of urea recorded at 298 K and 78 K.

Temperature, K		Fe Site *	298				78			
Sample	Subspectrum		Δ **	Δ	Γ_{exp}	S	δ	Δ	Γ_{exp}	S
			mm/s			%	mm/s			%
FH NP	1	Fe1	0.35 ± 0.02	0.92 ± 0.08	0.52 ± 0.02	60 ± 17	0.45 ± 0.01	0.91 ± 0.09	0.54 ± 0.02	71 ± 18
	2	Fe2	0.39 ± 0.01	0.57 ± 0.03	0.34 ± 0.05	23 ± 16	0.47 ± 0.01	0.54 ± 0.03	0.34 ± 0.06	23 ± 17
	3	Fe3	0.26 ± 0.04	0.54 ± 0.04	0.38 ± 0.03	17 ± 7	0.33 ± 0.07	0.42 ± 0.08	0.38 ± 0.10	6 ± 3
FH NP + urea	1	Fe1	0.35 ± 0.01	0.92 ± 0.09	0.50 ± 0.02	60 ± 18	0.45 ± 0.01	0.89 ± 0.07	0.52 ± 0.02	68 ± 14
	2	Fe2	0.38 ± 0.01	0.57 ± 0.02	0.33 ± 0.05	24 ± 18	0.47 ± 0.01	0.55 ± 0.03	0.34 ± 0.05	23 ± 15
	3	Fe3	0.27 ± 0.05	0.51 ± 0.06	0.39 ± 0.03	17 ± 7	0.38 ± 0.06	0.47 ± 0.06	0.38 ± 0.05	9 ± 8

* according to the designations reported in [65]; ** δ, isomer shift; Δ, quadrupole splitting; Γexp, line width; S, relative area of a subspectrum.

Two doublets with the room-temperature isomeric shift within 0.35–0.39 mm/s range were ascribed to the Fe^{+3} ions in the octahedral oxygen environment [65]. The doublet with the highest relative area has an isomeric shift of 0.35 mm/s and the largest quadrupole splitting (0.92 mm/s) (Table 1, subspectrum 1). It was designated as Fe^{3+} ions within the $\{Fe(O,OH)_6\}$ octahedra connected into layers referring to **Fe1** sites as described in [66]. Subspectrum 2 (Table 1) with the largest isomeric shift (0.39 mm/s) and a quadrupole splitting of 0.57 mm/s corresponds to Fe^{3+} ions in "isolated" oxygen octahedra was designated as **Fe2** sites as assigned in [66]. Intercorrelation, which can be clearly seen between the values of the quadrupole splitting and the width of the resonance lines of subspectra 1 and 2 (Table 1) has been reported elsewhere [67]. This indicates that the oxygen-containing molecular/ion species ($H_2O/OH^-/O^{2-}$), which surround iron atoms in ferrihydrite lattice, make a partial contribution to the Mössbauer parameters related to their dynamic properties and electromagnetic interactions.

The third doublet with the lowest relative area had the smallest quadrupole splitting (0.54 mm/s) and isomeric shift (0.26 mm/s), which corresponds to Fe^{3+} ions in a tetrahedral oxygen environment [65]. A small quadrupole splitting of this doublet indicates a higher symmetry of the environment (leading to a smaller electric field gradient for the corresponding iron atoms) and associates subspectrum 3 (Table 1) with Fe^{3+} ions in the **Fe3** position [66]. The ratio of subspectrum areas in the room-temperature spectrum is close to the theoretically expected one from the structural data: **Fe1**:**Fe2**:**Fe3** = 60:20:20 [68]. The observed change in this ratio at 78 K (Table 1) may be indicative of the deformation of the crystal lattice, which causes the consequent change in the Mössbauer factor of the corresponding iron atoms. Of interest is that the Fe ions in tetrahedral positions are rarely identified in ultra-dispersed ferrihydrite samples by room-temperature Mössbauer spectroscopy (e.g., compared with the reported data [18]). This is only possible for the ferrihydrite species with higher crystallinity, which might be the case in this study. It is feasible given that the synthesis of the FH sample was conducted at pH 10, thus causing the higher hydrolysis rate of Fe precursor as compared to that at pH 9 described by Cieschi et al. [18]. The quadrupole splitting and line widths of all the subspectra are temperature-independent (Table 1). This suggests the absence of magnetic ordering in the temperature range studied, which indicates rather small iron-containing particles [69]. The Mössbauer spectra of the FH sample treated with urea before the foliar application are shown in Figure 2.

The probability distribution functions for the isomeric shifts and quadrupole splitting were also fitted with three peaks, however the peak positions and widths of all modes increased markedly (Figure 2c,d). This is indicative of an increased relative content of inhomogeneities in the local environment of Fe^{3+} ions, e.g., some surface etching of the NPs after the addition of urea. Meanwhile, the fitting parameters of the experimental spectra of FH nanoparticles in the presence and absence of urea (Figure S2a,b) remain the same within the measurement accuracy (Table 1). Summarizing the Mössbauer data, it can be concluded that the synthesized FH nanofertilizer contains small ferrihydrite NPs of enhanced crystallinity as compared to the previously reported analogues synthesized at pH 9 [18]. Addition of urea does not significantly change the state of ferrihydrite NPs leading to a slight increase in the heterogeneity of the local environment of Fe^{3+} atoms.

3.2. Foliar Application of the FH Iron Source to Wheat Plants: Iron Uptake and its Physical-Chemical Justification

The obtained FH iron source was applied as a foliar spray to the iron-deficient wheat plants and compared with the positive control, Fe-EDTA treatment, and with the blank treatments using distilled water and the parent potassium humate. All treatments contained urea (0.2% wt.) as an effective adjuvant that increases the translocation of iron from the leaf surface into the shoot interior by improving permeation of ionic solutes from the water-based solutions into the aqueous pores in leaf cuticles [57,58]. After 7 days of cultivation, the wheat shoots were separated from the roots,

thoroughly washed with Brij/HCl solution, as suggested by Rodríguez-Lucena et al. [57] to ensure the removal of IONPs, which did not penetrate the leave pores, from the leaf surface. The content of iron in the leaves after the treatments are shown in Figure 3.

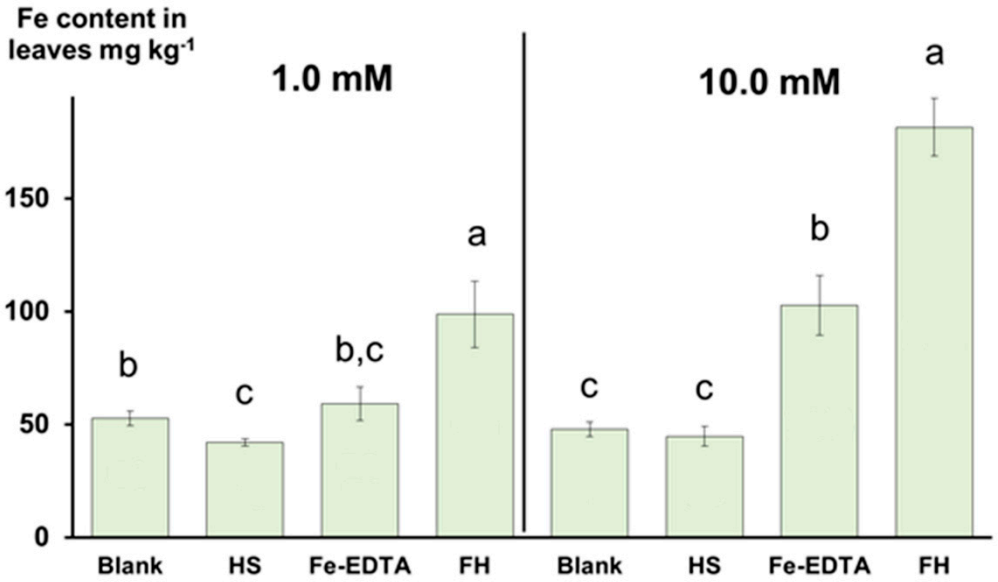

Figure 3. Iron content in the wheat leaves after foliar application of the iron-sources: ferrihydrite (FH) and ferric ammonium salt of ethylenediaminetetraacetic acid (Fe-EDTA), and control solutions: triple-distilled water (blank) and potassium humate (HS). The iron concentrations in the fertilizer sprays were 1.0 mM (left panel) and 10.0 mM (right panel). All treatments, except for the blank, contained urea adjuvant (0.2% wt.). The bars represent the standard deviation ($n = 4$). The columns marked with different letters are significantly different at $p < 0.05$ according to the least significant difference (LSD) test.

The use of 1 mM Fe solutions resulted in the higher iron content in the leaves in both the case of the FH sample and Fe-EDTA, moreover, the increase in the FH sample was larger than the Fe-EDTA sample (left panel of Figure 3). The treatment using the higher Fe dosage (10 mM) gave even more impressive results (right panel of Figure 3): in the case of the FH sample, the content of Fe in the leaves was 280% of the control (distilled-water treated leaves), whereas in the case of Fe-EDTA the corresponding increase was 115% of the control. Thus, the FH treatment was ca. 70–75% more efficient compared to Fe-EDTA at the higher concentration used in this study. The potassium humate treatment did not increase Fe content in the leaves as compared to the blank experiments. The data on the iron content in the shoot-washing solutions corroborate the obtained results: for both concentrations (1 and 10 mM), consistently higher iron content was observed for Fe-EDTA and a lower content was found for FH. So, the solution used to wash the leaves treated with 1 mM Fe-EDTA and FH spray contained 55 ± 13 and 12 ± 1 $\mu g \cdot L^{-1}$ of Fe, respectively (Table S1, Supplementary Materials). The same trend was observed for the treatment with 10 mM Fe: an iron content of 400 ± 150 and 100 ± 30 $\mu g \cdot L^{-1}$, were found in the shoot-washing solution used in the Fe-EDTA and FH treatments, respectively. Of importance is that almost no iron (significantly below 10 $\mu g \cdot L^{-1}$) was found in the distilled water washing solution used after Brij 35/HCl washing of the leaves treated with FH spray at concentrations of 1- and 10-mM Fe (Table S1, Supplementary Materials). The higher Fe content in the washed leaves and the lower iron content in the "after-treatment" washing solutions for the FH sample, as well as the opposite trend for the Fe-EDTA treatment suggest that there was higher penetration of IONPs in the leaves in the case of the FH sample compared to Fe-EDTA.

Along with the iron content, we measured the dry biomass of the shoots of the plants treated with the iron sources under study. The results are given in Figure 4. None of the treatments resulted in a statistically significant increase in shoot biomass. Our results are consistent with data obtained by Bastani et al. [70] who studied the effects of nano and bulk Fe complex (Fe(III)-EDTA) on

hydroponically-grown Fe-deficient tobacco (*Nicotiana rustica* L.). They demonstrated that the plant biomass was not affected by Fe foliar fertilization one week after treatment, although a statistically significant increase in iron content was observed. This is due to the lag period in the plants' response to the iron supply. The increase in the soil plant analysis development (SPAD) values related to chlorophyll content only begins 4–5 days after treatment [70], and in general, ten days are believed to be enough to see the re-greening of Fe-deficient plants after Fe foliar fertilization [71]. This is why the obtained data do not provide definite confirmation of the participation of the up taken iron in the relevant physiological processes. We can only comment on the corresponding trend. More extended studies are needed and more sensitive parameters should be measured (e.g., the photosynthetic activity of the plants).

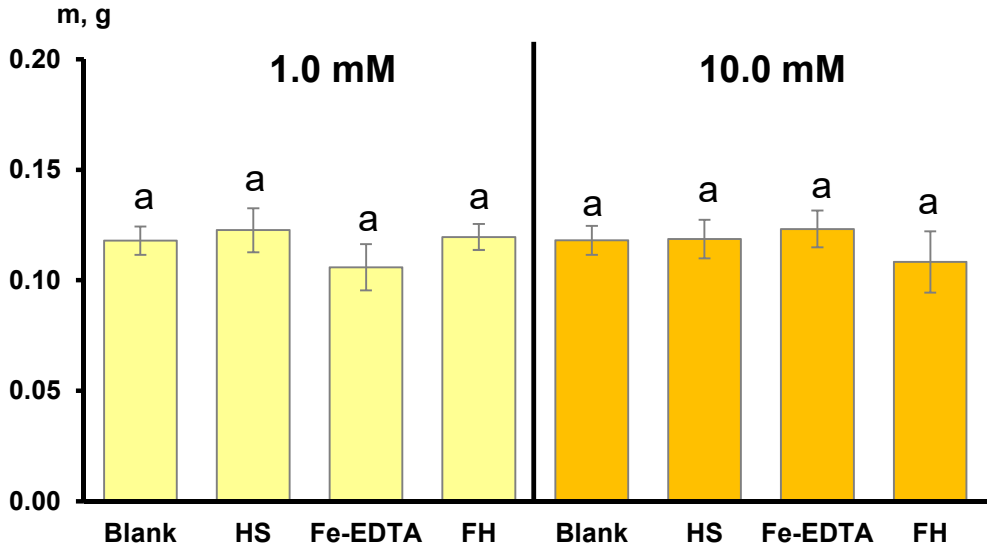

Figure 4. Dry biomass of the wheat shoots after foliar application of the iron-sources: ferrihydrite (FH) and Fe-EDTA, and control solutions: triple-distilled water (blank) and potassium humate (HS). The iron concentration in the fertilizer sprays was 1.0 mM (highlighted in yellow) and 10.0 mM (highlighted in orange). The bars represent the standard deviation (n = 5). The columns marked with different letters are significantly different at $p < 0.05$ according to LSD test.

To exploring the physical-chemical phenomena that underlie the observed increase in Fe uptake by wheat leaves after the FH spray as compared to the Fe-EDTA, we measured the surface tension of the HS solution and of both the iron-containing solutions applied for foliar fertilization. We also measured the contact angle of the corresponding spray droplets on the wheat leaves. We wanted to investigate whether the observed enhancement in Fe uptake was connected to the surface activity of HS, which could the lower surface tension of the urea-FH solution. This seemed feasible given that the HS sample used in this study had about 40% of C atoms in the hydrophilic functional groups, and the other 60% of C atoms in the hydrophobic carbon skeleton. The results obtained for the surface tension and contact angle are shown in Table 2 and Figure 5, respectively.

Table 2. Contact angles of the foliar spray droplets deposited on the surface of the wheat leaf and the surface tension of the corresponding solution.

Solution *	Surface Tension, mN/m (at 20 °C)	Contact Angle, ° (at 20 °C)
distilled water	73.6 ± 0.4 $^{b, c}$	110.2 ± 0.2 ^{a} **
solution of HS	73.7 ± 0.1 ^{b}	93.3 ± 0.4 ^{c}
Fe-EDTA	74.2 ± 0.2 ^{a}	95.2 ± 0.4 ^{b}
FH	73.2 ± 0.1 ^{c}	87.0 ± 0.5 ^{d}

* all solutions contained urea adjuvant (0.2% wt.), HS—potassium humate, FH—ferrihydrite; ** ± stands for a standard deviation for the surface tension (n = 5) and contact angle (n = 6). Values with different letters within a column are significantly different at $p < 0.05$

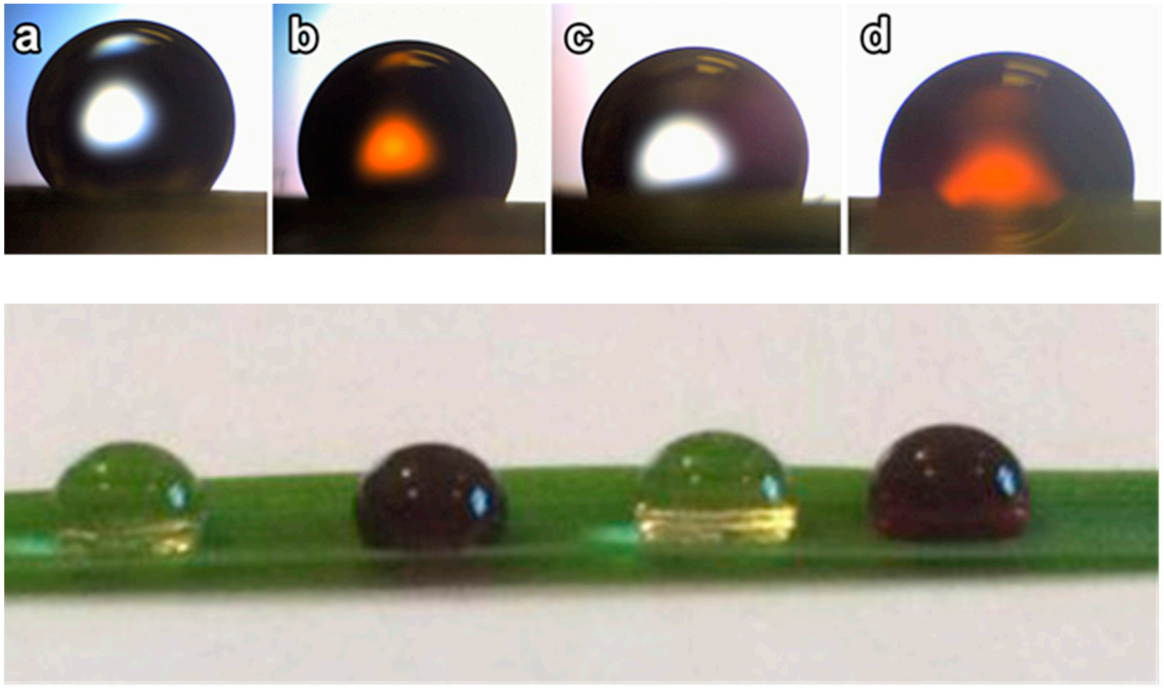

Figure 5. Images of the foliar spray droplets deposited on the surface of wheat leaf: (**a**) triple-distilled water; (**b**) HS (solution of potassium humate); (**c**) Fe-EDTA; (**d**) ferrihydrite nanoparticles (FH). All the solutions contained urea adjuvant (0.2% wt.). The image in the bottom row presents the total view of the droplets deposited on the surface of the wheat leaf.

Table 2 shows that in the presence of 0.2% urea, all tested solutions had a surface tension similar to distilled water. At the same time, the FH solution exhibited a lower (87°) contact angle on the surface of wheat leaf (Figure 5) as compared to Fe-EDTA (95.2°) and compared to both controls (water and humate solution). The FH solution showed the smallest contact angle, which resulted in the highest wettability of wheat leaves among all of the tested solutions. Of particular interest is that the contact angle for the FH solution was lower than that of the HS solution of the same concentration (Figure 5, Table 2). This observation agrees well with the report by Harikrishnan et al. [46] on enhanced wettability of hydrophobic and hydrophilic surfaces by complex fluids containing both surfactants and nanoparticles as compared to particle-free surfactant solutions. A study on emulsification [47] has shown that the addition of particles to a surfactant-stabilized emulsion results in the appearance of a small population of large drops due to coalescence, possibly by bridging of adsorbed particles. The addition of surfactant to a particle-stabilized emulsion surprisingly led to increased coalescence as well [47]. In our study, the larger drops, which were observed for the FH solution, might result from the higher wettability of the leaf surface due to accumulation of nanoparticles on the droplet/leaf surface. Since only residual iron from the IONPs spray was found in the after-treatment washing solution, it was assumed that the major portion had entered the leaf through its different-sized pores (stomatal pores, pores in the cell walls, etc.). Given that HS can promote the physiological mechanisms involved in Fe acquisition acting at the transcriptional and post-transcriptional level [72], the observed increased uptake of iron NPs stabilized by HS might be an eco-friendly and affordable tool for biofortification of crops, in particular, of wheat and rice.

4. Conclusions

In this study, ultrasmall ferrihydrite nanoparticles (with a mean size of 2.5 ± 0.3 nm) stabilized by potassium humate (HS) were synthesized and used in the form of a spray as an iron source for foliar application on wheat plants (*Triticum aestivum L.*) grown under iron-deficient conditions. This resulted in a 70–75% higher iron content in washed and dried wheat shoots compared to a coordination complex of ferric ions and ethylenediaminetetraacetic acid (Fe-EDTA). The higher uptake of iron from the ferrihydrite (FeH) stabilized with HS was related to the enhanced wettability of the wheat leaves. The obtained results are promising with regard to developing humic-stabilized nanofertilizers. Additional benefits are provided by the eco-friendly properties and plentiful resources of humic substances.

Supplementary Materials: The following are available online at www.mdpi.com/2073-4395/10/12/1891/s1, Table S1: Iron content in the solutions used to wash the wheat shoots after foliar treatments with humics-based nanofertilizer and control/blank preparations ($\mu g \cdot L^{-1}$).

Author Contributions: Conceptualization, I.V.P. and A.Y.P.; methodology, A.Y.P., N.A.K., M.M.Z., and I.V.P.; software, D.A.P., V.A.L., A.I.K.; validation, M.M.Z., D.S.V., formal analysis, M.M.Z., D.S.V., V.A.L., A.I.K., A.M.P., and O.Z.; resources, A.Y.P., D.S.V., N.A.K., V.A.L., D.A.P., A.M.P., O.Z.; writing—original draft preparation, M.M.Z., A.Y.P., D.A.P., D.S.V. and I.V.P; funding acquisition, I.V.P. All authors have read and agreed to the published version of the manuscript.

Funding: This study was funded by the Russian Foundation for Basic Research, project 18-29-25065: Synthesis of nanoferrihydrite and its characterization, and the Russian Science Foundation, project 16-14-00167: Vegetation experiments and Fe-content analysis.

Conflicts of Interest: The authors declare no conflict of interest

References

1. Mengel, K.; Kirkby, E.A.; Kosegarten, H.; Appel, T. *Iron. Principles of Plant Nutrition*; Springer: Dordrecht, Germany, 2001; pp. 553–571, doi:10.1007/978-94-010-1009-2_13.
2. Pérez-Labrada, F.; Benavides-Mendoza, A.; Juárez-Maldonado, A.; Solís-Gaona, S.; González-Morales, S. Organic acids combined with Fe-chelate improves ferric nutrition in tomato grown in calcisol soil. *J. Soil. Sci. Plant Nutr.* **2020**, *20*, 673–683, doi:10.1007/s42729-019-00155-3.
3. Cantera, R.G.; Zamarreño, A.M.; García-Mina, J.M. Characterization of commercial iron chelates and their behavior in an alkaline and calcareous soil. *J. Agric. Food Chem.* **2002**, *50*, 7609–7615, doi:10.1021/jf025745y.
4. Colombo, C.; Palumbo, G.; He, J.Z.; Pinton, R.; Cesco, S. Review on iron availability in soil: Interaction of Fe minerals, plants, and microbes. *J. Soils Sediments* **2014**, *14*, 538–548, doi:10.1007/s11368-013-0814-z.
5. Kulikova, N.A.; Polyakov, A.Y.; Lebedev, V.A.; Abroskin, D.P.; Volkov, D.S.; Pankratov, D.A.; Klein, O.I.; Senik, S.V.; Sorkina, T.A.; Garshev, A.V.; et al. Key roles of size and crystallinity of nanosized iron hydr(oxides) stabilized by humic substances in iron bioavailability to plants. *J. Agric. Food Chem.* **2017**, *65*, 11157–11169, doi:10.1021/acs.jafc.7b03955.
6. Rui, M.; Ma, C.; Hao, Y.; Guo, J.; Rui, Y.; Tang, X.; Zhao, Q.; Fan, X.; Zhang, Z.; Hou, T.; et al. Iron oxide nanoparticles as a potential iron fertilizer for peanut (*Arachis hypogaea*). *Front. Plant Sci.* **2016**, *7*, 815, doi:10.3389/fpls.2016.00815.
7. Schwertmann, U.; Fechter, H. The point of zero charge of natural and synthetic ferrihydrites and its relation to adsorbed silicate. *Clay Miner.* **1982**, *17*, 471–476, doi:10.1180/claymin.1982.017.4.10.
8. Sebastian, A.; Nangia, A.; Prasad, M.N.V. Carbon-bound iron oxide nanoparticles prevent calcium-induced iron deficiency in *Oryza sativa* L. *J. Agric. Food Chem.* **2017**, *65*, 557–564, doi:10.1021/acs.jafc.6b04634.
9. Illés, E.; Tombácz, E. The effect of humic acid adsorption on pH-dependent surface charging and aggregation of magnetite nanoparticles. *J. Colloid Interface Sci.* **2006**, *295*, 115–123, doi:10.1016/j.jcis.2005.08.003.
10. Vodyanitskii, Y.N. Iron hydroxides in soils: A review of publications. *Eurasian Soil. Sci.* **2010**, *43*, 1244–1254, doi:10.1134/S1064229310110074.
11. Chekanova, A.E.; Sorkina, T.A.; Dubov, A.L.; Nikiforov, V.N.; Davydova, G.A.; Selezneva, I.I.; Goodilin, E.A.; Trusov, L.A.; Korolev, V.V.; Aref'ev, I.M.; et al. New environmental nontoxic agents for the

preparation of core-shell magnetic nanoparticles. *Mendeleev Commun.* **2009**, *19*, 72–74, doi:10.1016/j.mencom.2009.03.006.

12. Colombo, C.; Palumbo, G.; Sellitto, V.M.; Cho, H.G.; Amalfitano, C.; Adamo, P. Stability of coprecipitated natural humic acid and ferrous iron under oxidative conditions. *J. Geochem. Explor.* **2015**, *151*, 50–56, doi:10.1016/j.gexplo.2015.01.003.
13. Wang, P.; Wang, J.; Zhang, H.; Dong, Y.; Zhaqng, Y. The role of iron oxides in the preservation of soil organic matter under long-term fertilization. *J. Soils Sediments* **2019**, *19*, 588–598, doi:10.1007/s11368-018-2085-1.
14. Kovács, K.; Czech, V.; Fodor, F.; Solti, A.; Lucena, J.J.; Santos-Rosell, S.; Hernández-Apaolaza, L. Characterization of Fe–leonardite complexes as novel natural iron fertilizers. *J. Agric. Food Chem.* **2013**, *61*, 12200–12210, doi:10.1021/jf404455y.
15. Pankratov, D.A.; Anuchina, M.M. Nature-inspired synthesis of magnetic non-stoichiometric Fe_3O_4 nanoparticles by oxidative in situ method in a humic medium. *Mater. Chem. Phys.* **2019**, *231*, 216–224, doi:10.1016/j.matchemphys.2019.04.022.
16. Polyakov, A.Y.; Goldt, A.E.; Sorkina, T.A.; Perminova, I.V.; Pankratov, D.A.; Goodilin, E.A.; Tretyakov, Y.D. Constrained growth of anisotropic magnetic δ-FeOOH nanoparticles in the presence of humic substances. *Cryst. Eng. Comm.* **2012**, *14*, 8097–8102, doi:10.1039/c2ce25886b.
17. Chassapis, K.; Roulia, M.; Nika, G. Fe(III)–humate Complexes from Megalopolis Peaty Lignite: A novel eco-friendly fertilizer. *Fuel* **2010**, *89*, 1480–1484, doi:10.1016/j.fuel.2009.10.005.
18. Cieschi, M.T.; Polyakov, A.Y.; Lebedev, V.A.; Volkov, D.S.; Pankratov, D.A.; Veligzhanin, A.A.; Perminova, I.V.; Lucena, J.J. Eco-friendly iron-humic nanofertilizers synthesis for the prevention of iron chlorosis in soybean (*Glycine max*) grown in calcareous soil. *Front. Plant Sci.* **2019**, *10*, 413, doi:10.3389/FPLS.2019.00413.
19. Cieschi, M.T.; Lucena, J.J. Iron and humic acid accumulation on soybean roots fertilized with leonardite iron humates under calcareous conditions. *J. Agric. Food Chem.* **2018**, *66*, 13386–13396, doi:10.1021/acs.jafc.8b04021.
20. Smith, A.M.; Gilbertson, L.M. Rational ligand design to improve agrochemical delivery efficiency and advance agriculture sustainability. *ACS Sustain. Chem. Eng.* **2018**, *6*, 13599–13610, doi:10.1021/acssuschemeng.8b03457.
21. Raliya, R.; Saharan, V.; Dimkpa, C.; Biswas, P. Nanofertilizer for precision and sustainable agriculture: Current state and future perspectives. *J. Agric. Food Chem.* **2018**, *66*, 6487−6503.
22. Achari, G.A.; Kowshik, M. Recent developments on nanotechnology in agriculture: Plant mineral nutrition, health, and interactions with soil microflora. *J. Agric. Food Chem.* **2018**, *66*, 8647−8661.
23. Khush, G.S.; Lee, S.; Cho, J. Biofortification of crops for reducing malnutrition. *Plant Biotechnol. Rep.* **2012**, *6*, 195–202.
24. Bala, R.; Kalia, A.; Dhaliwal, S.S. Evaluation of efficacy of ZnO nanoparticles as remedial zinc nanofertilizer for rice. *J. Soil. Sci. Plant Nutr.* **2019**, *19*, 379–389, doi:10.1007/s42729-019-00040-z.
25. Bouis, H.E. *Food Fortification in a Globalized World. Biofortification: An Agricultural Tool to Address Mineral and Vitamin Deficiencies*; Academic Press: Cambridge, MA, USA, 2018; pp. 69–81, doi:10.1016/B978-0-12-802861-2.00007-9.
26. Duhan, J.S.; Kumar, R.; Kumar, N.; Kaur, P.; Nehra, K.; Duhan, S. Nanotechnology: The new perspective in precision agriculture. *Biotechnol. Rep.* **2017**, *15*, 11–23, doi:10.1016/j.btre.2017.03.002.
27. Garcia-Casal, M.N.; Peña-Rosas, J.P.; Pachón, H.; De-Regil, L.M.; Centeno Tablante, E.; Flores-Urrutia, M.C. Staple crops biofortified with increased micronutrient content: Effects on vitamin and mineral status, as well as health and cognitive function in the general population. *Cochrane Database Syst. Rev.* **2016**, *8*, CD012311, doi:10.1002/14651858.CD012311.
28. Garg, M.; Sharma, N.; Sharma, S.; Kapoor, P.; Kumar, A.; Chunduri, V.; Arora, P. Biofortified crops generated by breeding, agronomy, and transgenic approaches are improving lives of millions of people around the world. *Front. Nutr.* **2018**, *5*, 12, doi:10.3389/fnut.2018.00012.
29. Hassanpouraghdam, M.B.; Mehrabani, L.V.; Tzortzakis, N. Foliar application of nano-zinc and iron affects physiological attributes of *Rosmarinus officinalis* and quietens NaCl salinity depression. *J. Soil Sci. Plant Nutr.* **2020**, *20*, 335–345, doi:10.1007/s42729-019-00111-1.
30. Li, P.; Li, L.; Du, Y.; Hampton, M.A.; Nguyen, A.V.; Huang, L.; Rudolph, V.; Xu, Z.P. Potential foliar fertilizers with copper and zinc dual micronutrients in nanocrystal suspension. *J. Nanoparticle Res.* **2014**, *16*, 2669, doi:10.1007/s11051-014-2669-7.

31. Raliya, R.; Nair, R.; Chavalmane, S.; Wang, W.N.; Biswas, P. Mechanistic evaluation of translocation and physiological impact of titanium dioxide and zinc oxide nanoparticles on the tomato (*Solanum lycopersicum* L.) plant. *Metallomics* **2015**, *7*, 1584–1594.
32. Alidoust, D.; Isoda, A. Effect of γ-Fe_2O_3 nanoparticles on photosynthetic characteristic of soybean (*Glycine max* (L.) Merr.): Foliar spray versus soil amendment. *Acta Physiol. Plant* **2013**, *35*, 3365–3375.
33. Wang, W.N.; Tarafdar, J.C.; Biswas, P. Nanoparticle synthesis and delivery by an aerosol route for watermelon plant foliar uptake. *J. Nanoparticle Res.* **2013**, *15*, 1417, doi:10.1007/s11051-013-1417-8.
34. Wei, Y.; Shohag, M.J.; Yang, X.; Yibin, Z. Effects of foliar iron application on iron concentration in polished rice grain and its bioavailability. *J. Agric. Food Chem.* **2012**, *60*, 11433–11439.
35. Aciksoz, S.B.; Yazici, A.; Ozturk, L.; Cakmak, I. Biofortification of wheat with iron through soil and foliar application of nitrogen and iron fertilizers. *Plant Soil* **2011**, *349*, 215–225.
36. Delfani, M.; Baradarn Firouzabadi, M.; Farrokhi, N.; Makarian, H. Some physiological responses of black-eyed pea to iron and magnesium nanofertilizers. *Commun. Soil Sci. Plant Anal.* **2014**, *45*, 530–540, doi:10.1080/00103624.2013.863911.
37. Fang, Y.; Wang, L.; Xin, Z.; Zhao, L.; An, X.; Hu, Q. Effect of foliar application of zinc, selenium, and iron fertilizers on nutrients concentration and yield of rice grain in China. *J. Agric. Food Chem.* **2008**, *56*, 2079–2084, doi:10.1021/jf800150z.
38. Pariona, N.; Martinez, A.I.; Hdz-García, H.M.; Cruz, L.A.; Hernandez-Valdes, A. Effects of hematite and ferrihydrite nanoparticles on germination and growth of maize seedlings. *Saudi J. Biol. Sci.* **2017**, *24*, 1547–1554, doi:10.1016/j.sjbs.2016.06.004.
39. Pinciroli, M.; Domínguez-Perles, R.; Abellán, Á.; Bultel-Poncé, V.; Durand, T.; Galano, J.M.; Ferreres, F.; Gil-Izquierdo, Á. Statement of foliar fertilization impact on yield, composition, and oxidative biomarkers in rice. *J. Agric. Food Chem.* **2019**, *67*, 597–605, doi:10.1021/acs.jafc.8b05808.
40. Zhang, T.; Sun, H.; Lv, Z.; Cui, L.; Mao, H.; Kopittke, P.M. Using synchrotron-based approaches to examine the foliar application of $ZnSO_4$ and ZnO nanoparticles for field-grown winter wheat. *J. Agric. Food Chem.* **2018**, *66*, 2572–2579.
41. Zhang, Y.; Shi, R.; Rezaul, K.M.; Zhang, F.; Zou, C. Iron and Zinc concentrations in grain and flour of winter wheat as affected by foliar application. *J. Agric. Food Chem.* **2010**, *58*, 12268–12274, doi:10.1021/jf103039k.
42. Sánchez Sánchez, A.; Oliver, M.; Cerdán, M.; Juárez, M.; Sánchez-Andreu, J.J. Influence of humic acids on iron uptake by Fe-deficient tomato plants. *Acta Hortic.* **2009**, *830*, 335–344, doi:10.17660/ActaHortic.2009.830.47.
43. Sánchez-Sánchez, A.; Sánchez-Andreu, J.; Juárez, M.; Jordá, J.; Bermúdez, D. Improvement of iron uptake in table grape by addition of humic substances. *J. Plant Nutr.* **2006**, *29*, 259–272, doi:10.1080/01904160500476087.
44. Nikolic, M.; Cesco, S.; Römheld, V.; Varanini, Z.; Pinton, R. Uptake of Iron (^{59}Fe) complexed to water-extractable humic substances by sunflower leaves. *J. Plant Nutr.* **2007**, *26*, 2243–2252, doi:10.1081/PLN-120024278.
45. Rodríguez-Lucena, P.; Tomasi, N.; Pinton, R.; Hernández-Apaolaza, L.; Lucena, J.J.; Cesco, S. Evaluation of ^{59}Fe-lignosulfonates complexes as Fe-sources for plants. *Plant Soil* **2009**, *325*, 53–63, doi:10.1007/s11104-009-0091-1.
46. Harikrishnan, A.R.; Dhar, P.; Agnihotri, P.K.; Gedupudi, S.; Das, S.K. Wettability of complex fluids and surfactant capped nanoparticle-induced quasi-universal wetting behavior. *J. Phys. Chem. B* **2017**, *121*, 6081–6095, doi:10.1021/acs.jpcb.7b02723.
47. Binks, B.P.; Desforges, A. Synergistic stabilization of emulsions by a mixture of surface-active nanoparticles and surfactant. *Langmuir* **2007**, *23*, 1098–1106.
48. Arab, D.; Kantzas, A.; Bryant, S.L. Nanoparticle stabilized oil in water emulsions: A critical review. *J. Petrol. Sci. Eng.* **2018**, *163*, 217–242.
49. Malqueen, P. Recent advances in agrochemical formulation. *Adv. Colloid Interface Sci.* **2003**, *106*, 83–107.
50. Kovalevskii, D.V.; Permin, A.B.; Perminova, I.V.; Petrosyan, V.S. Choice of the time of pulse delay for quantitative ^{13}C NMR spectroscopy of humic substances. *Mosc. Univ. Chem. Bull.* **2000**, *41*, 39–42.
51. Hertkorn, N.; Permin, A.; Perminova, I.; Kovalevskii, D.; Yudov, M.; Petrosyan, V.; Kettrup, A. Comparative analysis of partial structures of a peat humic and fulvic acid using one- and two-dimensional nuclear magnetic resonance spectroscopy. *J. Environ. Qual.* **2002**, *31*, 375–387, doi:10.2134/jeq2002.3750.

52. del Río, J.C.; González-Vila, F.J.; Martin, F.; Verdejo, T. Characterization of humic acids from low-rank coals by ^{13}C-NMR and pyrolysis-methylation. Formation of benzenecarboxylic acid moieties during the coalification process. *Org. Geochem.* **1994**, *22*, 885–891.
53. Perminova, I.V.; Frimmel, F.; Kovalevskii, D.; Abbt-Braun, G.; Kudryavtsev, A.; Hesse, S. Development of a predictive model for calculation of molecular weight of humic substances. *Water Res.* **1998**, *32*, 872–881.
54. Perminova, I.V.; Frimmel, F.H.; Kudryavtsev, A.V.; Kulikova, N.A.; Abbt-Braun, G.; Hesse, S.; Petrosyan, V.S. Molecular weight characteristics of humic substances from different environments as determined by size exclusion chromatography and their statistical evaluation. *Environ. Sci. Technol.* **2003**, *37*, 2477–2485, doi:10.1021/es0258069.
55. Nečas, D.; Klapetek, P. Gwyddion: An open-source software for SPM data analysis. *Open Phys.* **2012**, *10*, 181–188, doi:10.2478/s11534-011-0096-2.
56. Nardi, S.; Pizzeghello, D.; Gessa, C.; Ferrarese, L.; Trainotti, L.; Casadoro, G. A low molecular weight humic fraction on nitrate uptake and protein synthesis in maize seedlings. *Soil Biol. Biochem.* **2000**, *32*, 415–420.
57. Rodríguez-Lucena, P.; Ropero, E.; Hernández-Apaolaza, L.; Lucena, J.J. Iron supply to soybean plants through the foliar application of IDHA/Fe^{3+}: Effect of plant nutritional status and adjuvants. *J. Sci. Food Agric.* **2010**, *90*, 2633–2640, doi:10.1002/jsfa.4132.
58. Aciksoz, S.B.; Ozturk, L.; Yazici, A.; Cakmak, I. Inclusion of Urea in a ^{59}FeEDTA solution stimulated leaf penetration and translocation of ^{59}Fe within wheat plants. *Physiol. Plant* **2014**, *151*, 348–357, doi:10.1111/ppl.12198.
59. Colombo, C.; Iorio, E.; Liu, Q.; Jiang, Z.; Barrón, V. Iron oxide nanoparticles in soils: Environmental and agronomic importance. *J. Nanosci. Nanotechnol.* **2017**, *17*, 4449–4460, doi:10.1166/jnn.2017.14197.
60. Cornell, R.M.; Schwertmann, U. *The Iron Oxides: Structure, Properties, Reactions, Occurrences and Uses*; Wiley-VCH: Weinheim, Germany, 2003; pp. 201–220.
61. Zhu, B.S.; Jia, Y.; Jin, Z.; Sun, B.; Luo, T.; Kong, L.T.; Liu, J.H. A facile precipitation synthesis of mesoporous 2-line ferrihydrite with good fluoride removal properties. *RSC Adv.* **2015**, *5*, 84389–84397, doi:10.1039/C5RA15619J.
62. Chukhrov, F.V.; Zvyagin, B.B.; Gorshkov, A.I.; Yermilova, L.P.; Balashova, V.V. Ferrihydrite. *Int. Geol. Rev.* **1974**, *16*, 1131–1143, doi:10.1080/00206817409471766.
63. Combes, J.M.; Manceau, A.; Calas, G.; Bottero, J.Y. Formation of ferric oxides from aqueous solutions: A polyhedral approach by X-ray absorption spectroscopy: I. hydrolysis and formation of ferric gels. *Geochim. Cosmochim. Acta* **1989**, *53*, 583–594, doi:10.1016/0016-703790001-X.
64. Michel, F.M.; Ehm, L.; Antao, S.M.; Lee, P.L.; Chupas, P.J.; Liu, G.; Strongin, D.R.; Schoonen, M.A.A.; Phillips, B.L.; Parise, J.B. The structure of ferrihydrite, a nanocrystalline material. *Science* **2007**, *316*, 1726–1729, doi:10.1126/science.1142525.
65. Pankratov, D.A. Mössbauer study of oxo derivatives of iron in the Fe_2O_3-Na_2O_2 system. *Inorg. Mater.* **2013**, *50*, 82–89, doi:10.1134/s0020168514010154.
66. Michel, F.M.; Barron, V.; Torrent, J.; Morales, M.P.; Serna, C.J.; Boily, J.F.; Liu, Q.; Ambrosini, A.; Cismasu, A.C.; Brown, G.E. Ordered ferrimagnetic form of ferrihydrite reveals links among structure, composition, and magnetism. *Proc. Natl. Acad. Sci. USA* **2010**, *107*, 2787–2792, doi:10.1073/pnas.0910170107.
67. Pankratov, D.A.; Dolzhenko, V.D.; Ovchenkov, E.A.; Anuchina, M.M.; Severin, A.V. Properties of iron-containing nanohydroxyapatite-based composites. *Inorg. Mater.* **2017**, *53*, 115–124, doi:10.1134/S0020168517010125.
68. Hiemstra, T. Surface and mineral structure of ferrihydrite. *Geochim. Cosmochim. Acta* **2013**, *105*, 316–325, doi:10.1016/j.gca.2012.12.002.
69. Guyodo, Y.; Banerjee, S.K.; Penn, R.L.; Burleson, D.; Berquo, T.S.; Seda, T.; Solheid, P. Magnetic properties of synthetic six-line ferrihydrite nanoparticles. *Phys. Earth Planet Inter.* **2006**, *154*, 222–233, doi:10.1016/j.pepi.2005.05.009.
70. Bastani, S.; Hajiboland, R.; Khatamian, M.; Saket-Oskoui, M. Nano iron (Fe) complex is an effective source of Fe for tobacco plants grown under low Fe supply. *J. Soil Sci. Plant Nutr.* **2018**, *18*, 524–541.
71. Michel, L.; Beyá-Marshall, V.; Rombolà, A.D.; Pastenes, C.; Covarrubias, J.I. Evaluation of Fe-heme applications or intercropping for preventing iron deficiency in blueberry. *J. Soil Sci. Plant Nutr.* **2019**, *19*, 117–126, doi:10.1007/s42729-019-0017-9.

72. Zanin, L.; Tomasi, N.; Cesco, S.; Varanini, Z.; Pinton, R. Humic substances contribute to plant iron nutrition acting as chelators and biostimulants. *Front. Plant Sci.* **2019**, *10*, 675, doi:10.3389/fpls.2019.00675.